

Surface density: a new parameter in the fundamental metallicity relation of star-forming galaxies

Tetsuya Hashimoto,¹* Tomotsugu Goto,¹ and Rieko Momose¹

¹*Institute of Astronomy, National Tsing Hua University, 101, Section 2, Kuang-Fu Road, Hsinchu, 30013, Taiwan (R.O.C.)*

Accepted 2018 January 10. Received 2018 January 10; in original form 2017 August 6

ABSTRACT

Star-forming galaxies display a close relation among stellar mass, metallicity and star-formation rate (or molecular-gas mass). This is known as the fundamental metallicity relation (FMR) (or molecular-gas FMR), and it has a profound implication on models of galaxy evolution. However, there still remains a significant residual scatter around the FMR. We show here that a fourth parameter, the surface density of stellar mass, reduces the dispersion around the molecular-gas FMR. In a principal component analysis of 29 physical parameters of 41,338 star-forming galaxies, the surface density of stellar mass is found to be the fourth most important parameter. The new four-dimensional fundamental relation forms a tighter hypersurface that reduces the metallicity dispersion to 50% of that of the molecular-gas FMR. We suggest that future analyses and models of galaxy evolution should consider the FMR in a four-dimensional space that includes surface density. The dilution time scale of gas inflow and the star-formation efficiency could explain the observational dependence on surface density of stellar mass.

Key words: galaxies: fundamental parameters – formation

1 INTRODUCTION

The relation between stellar mass and gas-phase metallicity, which was discovered a decade ago, is one of the most fundamental relations for star-forming galaxies both in the local universe and at high redshifts (Tremonti et al. 2004; Erb et al. 2006). The gas-phase metallicity, here, is a measure of the relative amount of oxygen and hydrogen present. Many explanations for this relation have been proposed, including metal depletion by enriched gas outflow, which depends on the galactic gravitational well (Garnett 2002; Tremonti et al. 2004; Köppen et al. 2007; Brooks et al. 2007; Dalcanton 2007; Calura et al. 2009; Finlator & Davé 2008). Since its discovery, this relation has been developed into what is known as the fundamental metallicity relation (FMR) among stellar mass, metallicity and star-formation rate (SFR), defining a curved surface in the equivalent three-dimensional (3D) parameter space (Mannucci et al. 2010). In Mannucci et al. (2010), the large dispersion around the stellar-mass metallicity relation can be explained by the difference of SFRs of individual galaxies, which reduces the scatter significantly. Recent instances of the FMR based on large statistical samples of star-forming galaxies have dramatically advanced our understanding of galaxy evolution. For example, the negative correlation that exists between SFR and metallicity

in the FMR can be understood in the context of the inflow of metal-poor gas that directly dilutes the gas-phase metallicity and also triggers star formation (Mannucci et al. 2010; Forbes et al. 2014). The observed strength of the negative correlation between SFR and metallicity may depend on different metallicity calibration methods (Telford et al. 2016; Kashino et al. 2016) and different ways to be observed, i.e. single-fiber or integral-field observations (Sánchez et al. 2017; Barrera-Ballesteros et al. 2017).

There remains a significant residual scatter in metallicity beyond measurement error even after the SFR dependence is removed (Salim et al. 2014, 2015). This suggests that there could be an other factor which regulates metallicity of star-forming galaxies except for SFR. The possible fourth parameter following SFR could reduce the scatter around the 3D relation as the third parameter, SFR, reduced the dispersion around the mass-metallicity relation. The goal of this paper is finding out the fourth most important physical parameter of star-forming galaxies which reduces the scatter around the 3D relation. We describe the sample selection and present a brief summary of 29 physical parameters collected for individual galaxies in section 2. In section 3, we explain how to select candidates among 29 parameters. We examine actual tightnesses of fundamental relations defined by various combinations of candidate parameters in section 4. Our finding of the possible fourth most important parameter is shown in section 5. We present

* E-mail: tetsuya@phys.nthu.edu.tw

a comparison of the resulting metallicity dispersions around the fundamental relations with previous works in section 6. In section 7 we discuss possible physical interpretations of the fourth parameter. We finally summarize and conclude in section 8.

2 SAMPLE SELECTION

The galaxies in our sample were selected from the Sloan Digital Sky Survey (SDSS) Data Release 7 (Abazajian et al. 2009). We used the publicly available catalogue of emission-line fluxes produced in collaboration between the Max Planck Institute for Astrophysics (MPA) and Johns Hopkins University (JHU) (Kauffmann et al. 2003; Brinchmann et al. 2004; Salim et al. 2007). The criteria for selecting star-forming galaxies were based on previous research on the stellar-mass-metallicity relation (Kewley & Ellison 2008). A signal-to-noise ratio (S/N) of at least 8 was required in the strong optical emission lines of [O II] λ 3726, 3729, H β , [O III] λ 5007, H α , [N II] λ 6584 and [S II] λ 6717, 6731 for reliable estimates of metallicity and electron density. The median values of S/N of these emission lines in our sample are 15.5, 17.5, 32.7, 18.0, 81.5, 41.3, 28.4, and 21.4, respectively. This S/N limit on emission lines ensures accurate measurements of physical parameters but could lead to a biased sample. Galaxies with strong emission lines could be biased towards higher SFR and lower metallicity, which would enhance the dependence of metallicity on SFR (de los Reyes et al. 2015). This is probably because the emission-line fluxes are directly related to SFR and metallicity. Our present target of surface density of stellar mass was estimated from continuum fluxes, and it is independent of the emission lines. Therefore, the S/N criteria are unlikely to have an impact on our analysis, although the parameter range of metallicity may be biased to some extent. The redshift range was limited to 0.04-0.1. The lower redshift limit ensured at least 20% higher fibre covering fraction of the total photometric g' -band light as required for metallicity to approximate the global value (Kewley et al. 2005). The upper redshift limit is due to the fact that the SDSS sample of star-forming galaxies becomes incomplete at redshifts above 0.1 (Kewley et al. 2006). Host galaxies of active galactic nuclei (AGNs) were excluded by using the emission-line-ratio diagnostic diagram (i.e. a Baldwin-Phillips-Terlevich diagram (Baldwin et al. 1981)) and the AGN selection criteria (Kauffmann et al. 2003). The resulting sample contained 41,338 star-forming galaxies after removing duplicates in the emission-line catalogue. In summary, we used the following criteria to select star-forming galaxies.

- S/N > 8 for strong optical emission lines
- 0.04 < redshift < 0.1
- $\log([\text{O III}]\lambda 5007/\text{H}\beta) < 0.61/(\log([\text{N II}]\lambda 6584/\text{H}\alpha) - 0.05) + 1.3$

In total, 18 physical parameters of the sampled galaxies were compiled from various literatures, and a further 11 were calculated in this work. Note that 11 parameters include N2O3 index which is defined as $\text{N2O3} = \log([\text{N II}]\lambda 6584/\text{H}\alpha)/([\text{O III}]\lambda 5007/\text{H}\beta)$. This emission-line

ratio is linked to metallicity according to the calibration formula of $12 + \log(\text{O}/\text{H}) = 8.73 + 0.32 \times \text{N2O3}$ with a statistical uncertainty of ~ 0.1 dex (Pettini & Pagel 2004; Marino et al. 2013). Throughout this paper, we use N2O3 as an indicator of metallicity to avoid this large statistical uncertainty which is involved when N2O3 is converted to the actual value of metallicity.

We also note that 29 parameters contain not only single measurements but also their combinations such as molecular-gas mass which can be calculated from SFR and half-light radius assuming the Kennicutt-Schmidt law (Kennicutt 1998). The molecular-gas mass is mathematically equivalent to the combination of the SFR and half-light radius here. However the physical meaning of molecular-gas mass is different from SFR and half-light radius actually. It is possible for molecular-gas mass to be more important than SFR (or radius) itself according to underlying physical mechanism to regulate other parameters such as metallicity. Therefore we treat combinations as independent parameters.

The 29 parameters are summarised in Table 1 and details are in APPENDIX A.

3 PRINCIPAL COMPONENT ANALYSIS

Principal component analysis (PCA) is a useful method for investigating the relative contributions of individual parameters to the observed dispersion in a set of data. It involves constructing a new set of parametric axes PC1, PC2, ..., PC n that are ordered by decreasing contribution to the total dispersion and that are formed from linear combinations of the original parameters. These new axes are mutually perpendicular and not to change the original data distribution. To find a new fundamental parameter for the FMR, we carried out PCA on 41,338 star-forming galaxies selected from the SDSS Data Release 7 (Abazajian et al. 2009). We included 29 physical parameters categorised into six groups, namely, MASS, METAL, ACTIVITY, SIZE/MORPHOLOGY, ENVIRONMENT and OTHER (see Table 1 and APPENDIX A). The resulting ‘factor loadings’ are indicators of how strongly each original parameter contributes to the new axes (see APPENDIX B). The large absolute value of the factor loading indicates large contribution to the new PC axes. The same signs of factor loadings mean positive correlation between the parameters. Different signs show anti-correlation between the parameters.

In particular, the factor loadings of the parameters in the MASS, ACTIVITY and METAL groups show relatively high absolute values along the PC1 axis (Figure 1a). The archetypes of these three groups (i.e. stellar mass, SFR and N2O3, respectively) have the same sign along PC1, reflecting the well-known first-order stellar-mass-SFR and stellar-mass-metallicity relations. The main contributors to PC2 are the SIZE/MORPHOLOGY parameters. As for PC3, the ACTIVITY and METAL parameters show higher absolute values of factor loadings compared to those in the MASS group (Figure 1b). The factor loading of N2O3 is opposite in sign to the indicators of star formation, which suggests a general trend of negative correlation between the star-forming activity and metallicity such as the SFR-metallicity anti-correlation reported by Mannucci et al. (2010).

The aforementioned correlations, to some extent, repre-

sent known relations in the FMR (Mannucci et al. 2010). However, the distribution of 29 parameters in Figure 1 shows complex inter-relations between many parameters. Thus quantitative interpretations of individual PC axes are quite complicated.

To avoid the complexity in Figure 1, we adopt a criteria to select important parameters from this diversity based on the distance in the 3D space of factor loadings of PC1, PC2 and PC3 (instead of using values along each PCA axis). The PC1, PC2 and PC3 axes explain most ($\sim 70\%$) of the overall distribution of galaxies, suggesting the contribution from the fourth parameter to these three axes if it exists. Therefore the comprehensive contributions of the original parameters to the galactic distribution are indicated by the radial distances from the origin in the 3D space of the PC1, PC2 and PC3 factor loadings. The physical parameters in each categories are listed in Table 1 in order of the distance in PC1-3 factor loading space. The most important parameters in each group (i.e. the most distant parameters in the 3D factor-loading space) are stellar mass (MASS), N2O3 (METAL), molecular-gas mass (ACTIVITY), surface density of stellar mass (SIZE/MORPHOLOGY), dark-matter halo mass (ENVIRONMENT) and ionisation parameter (OTHERS). We conduct further exploration of these parameters as well as SFR and half-light radius, the latter two of which are included as existing references.

Of the remaining parameters, we note electron density, ionised-gas mass and metal mass as being outliers along PC4, which were calculated by using electron density (see APPENDIX A). However, unlike the parameters along PC3, the aforementioned three parameters are widely spread, implying a little correlation with other parameters such as stellar mass, N2O3, molecular-gas mass and surface density of stellar mass.

4 3D/4D MEDIAN SURFACES OF FUNDAMENTAL RELATIONS

In section 3, stellar mass, N2O3, molecular-gas mass, surface density of stellar mass, dark-matter halo mass and ionization parameter are selected as candidates of fundamental physical parameters of star-forming galaxies. In this section we calculate tightnesses of fundamental relations defined by various combinations of these candidate parameters to find out the fourth most important parameter which reduces the scatter around the 3D fundamental relation. We here performed additional PCAs for various 3D combinations of candidate parameters (not 29 in section 3) to carefully define the representative surface distributions of data points. Note that PCAs here are independent of the analysis in section 3 and performed only for the purpose of calculation of the representative surface in 3D space.

The data points are mostly spread out in the PC1-PC2 space because PC3 makes the smallest contribution to the total dispersion. This means that the median values along PC3 reflect the representative curved surface distribution of the data points. Therefore, to derive the 3D fundamental relation, we calculated the median distribution of data points along the PC3 in the PC parameter space. The PC1-PC2 space is split into grids in units of $\sigma_{PC1} \times \sigma_{PC2}$, where σ_{PC1} and σ_{PC2} are the dispersions of the data points along each

axis. A unit of five grid neighbours is used to calculate a local median surface. The offset of each data point is defined by the orthogonal distance from the closest median surface. We extended the same analysis to the four-dimensional (4D) fundamental relation by adding an extra dimension to the 3D one.

5 SURFACE DENSITY-N2O3 RELATION

Figure 2a shows the standard deviations around the median surfaces of the fundamental galactic relations defined by stellar mass, N2O3 and various choices for the third parameter. The standard deviations were calculated using orthogonal distances from the median surfaces in the standardised 3D parameter spaces so that the tightness of the different relations could be fairly compared with each other. A set of more fundamental parameters should construct a tighter relation according to the underlying physical mechanism of star-forming galaxies. The use of SFR as the third parameter corresponds to the conventional FMR and shows the second smallest scatter among the various choices for the third parameter (coloured dots in Figure 2a).

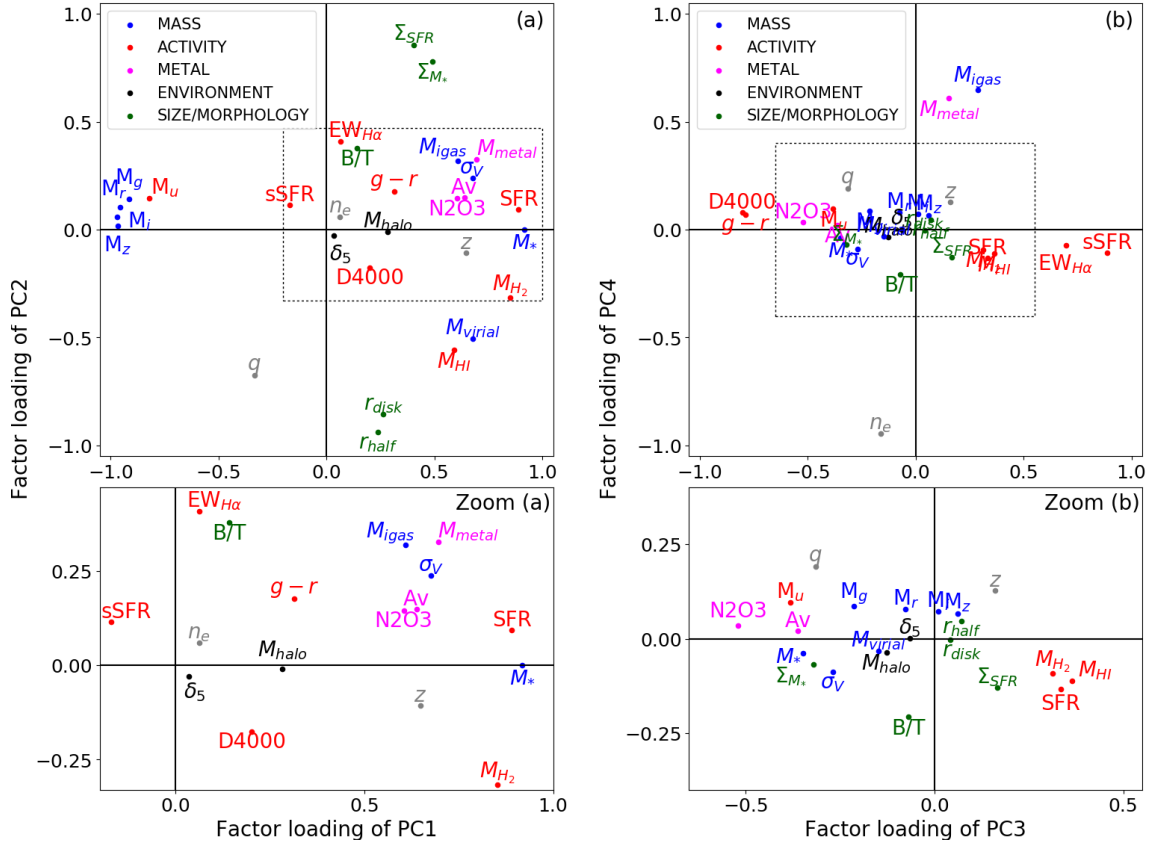
Recently, it has been suggested that molecular-gas mass is more fundamental than SFR as the third parameter (the former option is referred to hereinafter as the molecular-gas FMR) because of the large contribution of the molecular-gas mass to metallicity that is indicated from the fundamental plane of the galactic distribution (Bothwell et al. 2013, 2016b,a). Although it is beyond the scope of this paper to judge which is more important as the third parameter (SFR or molecular-gas mass), we attempted to estimate the molecular-gas mass by assuming the well-established Kennicutt-Schmidt law (Kennicutt 1998) that connects SFR and molecular-gas mass (see APPENDIX A). This is an indirect way to estimate the molecular-gas mass, but the alternative option of estimating it directly by CO observation is time-consuming and anyway is not feasible for the large sample used here (furthermore, the CO conversion factors are uncertain and could depend on metallicity (Wolfire et al. 2010; Feldmann et al. 2012; Schruba et al. 2012), which we wish to predict). In Figure 2a, the molecular-gas FMR actually results in slightly less scatter than does the conventional FMR, which may support the use of molecular-gas mass as the third fundamental parameter.

The standard deviation of the 3D relation defined by stellar mass, N2O3 and surface density of stellar mass (left green dot in Figure 2a) is not as small as that by using molecular-gas mass, confirming that molecular-gas mass is the third parameter. However, if surface density of stellar mass is incorporated into the molecular-gas FMR as an additional fourth parameter, the extent of galactic dispersion is indeed reduced (rightmost purple star in Figure 2a). The standard deviations around the molecular-gas FMR and this new 4D relation including surface density of stellar mass are separated into the triaxial components of stellar mass, N2O3 and molecular-gas mass in the standardised scale in Figure 2b. The reduction in dispersion by adding the fourth parameter is predominant in N2O3; the reductions in the other parameters are more moderate.

We suggest the correlation between surface density of stellar mass and N2O3 as the primary cause of the residual

Table 1. Summary of 29 parameters of SDSS star-forming galaxies, categorised into six groups (see APPENDIX A for details) in order of radial distance in the 3D space of the factor loadings of PC1, PC2 and PC3.

MASS		METAL		ACTIVITY	
M_*	Stellar mass	N2O3	Metallicity indicator	M_{H_2}	Molecular-gas mass
M_i	<i>i</i> -band absolute magnitude	M_{metal}	Metal mass in ionised gas	SFR	Star-formation rate
M_z	<i>z</i> -band absolute magnitude	Av	Dust extinction	M_u	<i>u</i> -band absolute magnitude
M_r	<i>r</i> -band absolute magnitude			sSFR	Specific star-formation rate
M_g	<i>g</i> -band absolute magnitude			M_{HI}	Atomic hydrogen gas mass
M_{virial}	Virial mass ($2r_{half}\sigma^2/G$)			<i>g-r</i>	Colour
σ	Velocity dispersion			D4000	Strength of 4000-Å break
M_{igas}	Ionised-gas mass			EW _{Hα}	Equivalent width of H α
SIZE/MORPHOLOGY		ENVIRONMENT		OTHER	
Σ_{M_*}	Surface density of M_*	M_{halo}	Dark-matter halo mass	q	[O III] λ 5007/[O II] λ 3727
r_{half}	<i>r</i> -band half-light radius	δ_5	Local galaxy number density	z	Redshift
Σ_{SFR}	Surface density of SFR			n_e	Electron density
r_{disk}	<i>r</i> -band disk radius				
B/T	Bulge-to-total fraction				

**Figure 1.** Factor loadings of principal components PC1, PC2, PC3 and PC4. The square of factor loading is an indicator of how strongly any original parameter contributes to the principal components. The same signs of factor loading means positive correlation between the parameters. Different signs show anti-correlation between the parameters. Colours show groupings of 29 parameters of star-forming galaxies. Dashed rectangular regions in the upper panels are magnified in the lower panels. The parameters are summarised in Table 1 (see APPENDIX A for details).

scatter around the molecular-gas FMR. This is confirmed clearly in Figure 3a, where we show the projected N2O3 offsets from the molecular-gas FMR as a function of surface density of stellar mass. Here the molecular-gas FMR means the median surface of the data distribution in the 3D space

of stellar-mass, N2O3 and molecular-gas mass, which is one of calculations described in section 4. The vertical axis is the orthogonal offset from the molecular-gas FMR projected on N2O3 axis.

Note that hereinafter all physical parameters are ex-

pressed in physical scales for reference to previous studies unless otherwise noted. In Figure 3a, galaxies are sampled into three different stellar-mass bins and a fixed molecular-gas mass (i.e. different gas mass fractions $f_{gas} = M_{H_2}/M_*$) to minimise the effects of stellar mass and molecular-gas mass on N2O3. High- f_{gas} galaxies show a negative correlation between the surface density of stellar mass and N2O3 offset, whereas low- f_{gas} galaxies show a positive relation within the N2O3 dispersion around the molecular-gas FMR. The vertical dynamic ranges of these correlation/anti-correlation are larger than the expected uncertainty of N2O3 offset measurements in our sample (~ 0.04 dex discussed in section 6).

N2O3 (not offset) as a function of surface density of stellar mass is shown in Figure 3b for the three galaxy samples. According to the molecular-gas FMR, the N2O3 of the samples should not show any surface-density dependence because of the fixed stellar mass and molecular-gas mass.

However, in Figure 3b, the three samples display the same trend, namely, a negative relation for high- f_{gas} galaxies and a positive relation of low- f_{gas} galaxies, which is consistent with Figure 3a. In Figure 3, it is not still clear whether stellar mass governs the relation, or f_{gas} does. To clarify this point, in Figure 4, we changed the f_{gas} with fixed stellar mass. These trends are also confirmed in Figure 4, which shows a more detailed breakdown of the galaxies into eight bins. Although there is no polynomial fit for the massive/high- f_{gas} bin (bottom right in the key) because the sample was too small, galaxies in the same range of stellar mass (the same line style) display different relations depending on f_{gas} . For the same f_{gas} (the same colour), galaxies with different stellar masses show similar dependencies. Therefore, the general trend of each surface-density-N2O3 relation depends on f_{gas} rather than on stellar mass or molecular-gas mass. These correlations underlying the molecular-gas FMR contribute to the dispersion around the 3D relation.

In relation to the fourth parameter, pioneering studies suggest a dependence on size of galaxy in the mass-metallicity relation (not the FMR) (Ellison et al. 2008; Brinbin & Harwit 2012; Yabe et al. 2014; Salim et al. 2014). A 4D relation among stellar mass, metallicity, SFR and ionisation parameter has also been reported (Nakajima & Ouchi 2014). Figure 1 confirms that these parameters show relatively high absolute values of factor loading. However, these values are still lower than that of surface density of stellar mass. In fact, as shown in Figure 2, the size and ionisation parameters do not construct the tightest relation in either 3D or 4D, which suggests that surface density of stellar mass is more fundamental. The present work is the first time that the relative dependence of the full FMR is shown quantitatively.

6 N2O3 DISPERSION AROUND THE 3D/4D RELATIONS

6.1 Observed N2O3 dispersion

It is well-known that different metallicity-calibration methods lead to different absolute values of metallicity (Kewley & Ellison 2008), which causes a large systematic error. A relative value of metallicity (e.g. dispersion or offset) can

be measured more accurately as long as the same method is used to calibrate the metallicity. The metallicity calibrations themselves have large statistical uncertainties, e.g. ~ 0.1 dex for PP04 method (Pettini & Pagel 2004; Marino et al. 2013). Thus uncertainty of ~ 0.1 dex is always involved when the emission-line ratio is converted to the metallicity. As long as N2O3 is adopted instead of the conversion to metallicity unit, we lose the information on actual values of metallicity of individual galaxies. However N2O3 still works statistically as an indicator of metallicity when we collect a large amount of sample.

The 3D standard deviation of the molecular-gas FMR corresponds to 0.07 dex in the projected N2O3 axis in the physical scale. The dispersion of 0.07 dex in N2O3 corresponds to 0.023 dex in PP04 metallicity calibration (Pettini & Pagel 2004), which is a much smaller deviation than those in previous works, i.e., ~ 0.05 dex (Mannucci et al. 2010; Telford et al. 2016; Sánchez et al. 2017; Barrera-Ballesteros et al. 2017). This is mainly due to the different method used here to estimate the dispersion around the relation. The orthogonal distance adopted here provides more reliable information on the tightness of each relation than does the distance along only the metallicity axis as used in previous works. In general, the projection of orthogonal distance is smaller than the distance calculated along an arbitrary axis. As a pure geometric effect, tilt of data distribution reduces the projected orthogonal distance by a factor of $(1 - \cos^2\theta)$ as a first-order approximation. The mass-N2O3 relation shows roughly $\theta=45$ degree in the standardized space which corresponds to factor of ~ 0.5 (see also Figure 7). Metallicity dispersion in our analysis divided by 0.5 is $0.023/0.5 = 0.046$ dex. This value is almost comparable to results of other works (~ 0.05 dex).

Figure 5 shows the peaked distribution of N2O3 offsets from the new 4D relation defined by stellar mass, N2O3, molecular-gas mass and surface density of stellar mass in comparison with the broad distribution of offsets from the molecular-gas FMR. N2O3 as measured by the emission-line diagnostic is clearly much better correlated with the predictions from the 4D fundamental relation than it is with those from the molecular-gas FMR. The corresponding N2O3 dispersion of the 4D relation is 0.034 dex, which is $\sim 50\%$ of the dispersion of the molecular-gas FMR (0.07 dex) in N2O3 axis.

6.2 Error budget

In principle, offset measurements in N2O3 axis around the 4D relation can be affected by the observational uncertainties on N2O3, stellar mass, molecular-gas mass and surface density of stellar mass regardless of the projection of the orthogonal distance (this paper) or offset measured along only N2O3 axis (adopted in previous studies). We here investigate how these four parameters affect on the N2O3 offset measurement.

The observational error of N2O3, $\delta N2O3$, is simply expressed as $\delta N2O3 = [(\delta \log [N II]\lambda 6584)^2 + (\delta \log H\alpha)^2 + (\delta \log [O III]\lambda 5007)^2 + (\delta \log H\beta)^2]^{1/2}$. Figure 6 is the normalised histogram of $\delta N2O3$ in our sample. The histogram peaks at $\delta N2O3 \sim 0.03$ dex and declines around $\delta N2O3 \sim 0.06$ which roughly corresponds to the selection limit of the sample. As mentioned in section 2, we imposed $S/N > 8$ for all

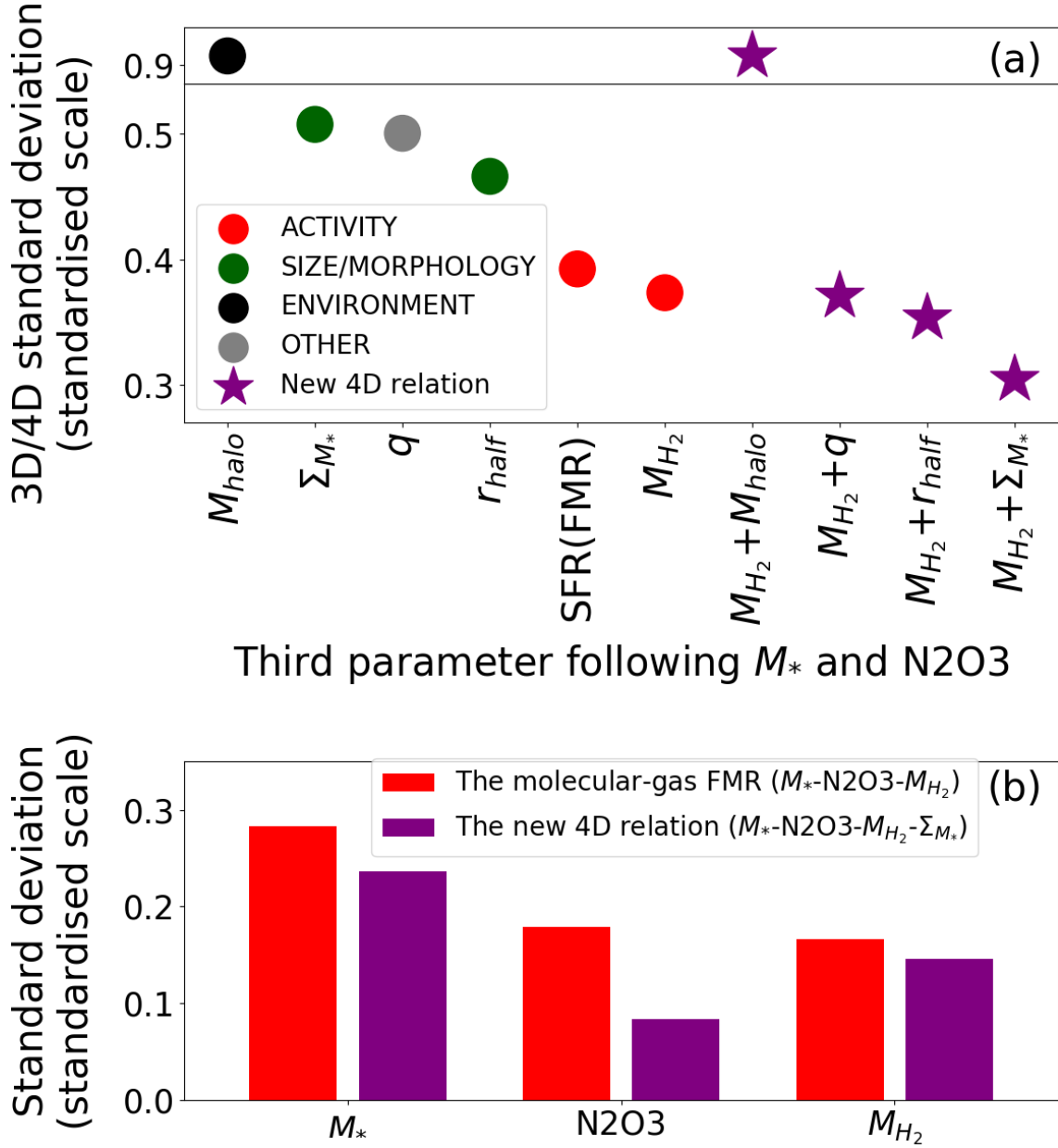


Figure 2. Standard deviations around fundamental relations in the standardised scale. (a), Standard deviations around fundamental relations in 3D parameter spaces defined by stellar mass, N2O3 and various third parameters (red, green, black and grey dots), also including 4D parameter spaces (purple stars). (b), Breakdown of standard deviations around the 3D and 4D relations (i.e. the molecular-gas FMR and the addition of the surface density of stellar mass) into triaxial components of stellar mass, N2O3 and molecular-gas mass.

of [O II] λ 3726, 3729, H β , [O III] λ 5007, H α , [N II] λ 6584 and [S II] λ 6717, 6731 lines on our sample. Therefore, the selection limit is determined by emission lines with relatively smaller S/N such as [O II] λ 3726, 3729 rather than N2O3.

The effects of uncertainties of molecular-gas mass and surface density of stellar mass on N2O3 offset are well below the typical value of N2O3 error (0.03 dex) as following arguments. The observational error of molecular-gas mass is likely dominated by the SFR error because we assume the Schmidt-Kennicutt law to estimate the molecular-gas mass (see APPENDIX A). The typical S/N of H α flux in our sample is 81.5 which corresponds to $\delta \log \text{SFR} = 0.0053$, where $\delta \log \text{SFR}$ is the observational error of $\log \text{SFR}$. Given the

SFR- Δ metallicity relation of star-forming galaxies with the fixed stellar mass of $\log M_* = 10$ (Mannucci et al. 2010), the uncertainty of 0.0053 dex in $\log \text{SFR}$ roughly corresponds to 0.003 dex uncertainty in N2O3. Based on the similar argument, the possible effect of the error of surface density of stellar mass is roughly estimated to be 0.003-0.005 dex in N2O3 according to the surface-density- Δ N2O3 relation at the fixed stellar mass and molecular-gas mass as shown in Figure 3a. In this calculation, we assumed that the uncertainty of the surface density of stellar mass is dominated by stellar-mass error which is typically $\delta \log M_* = 0.06 - 0.092$ in our sample depending on stellar mass according to the error estimates provided by MPA/JHU catalogue). These

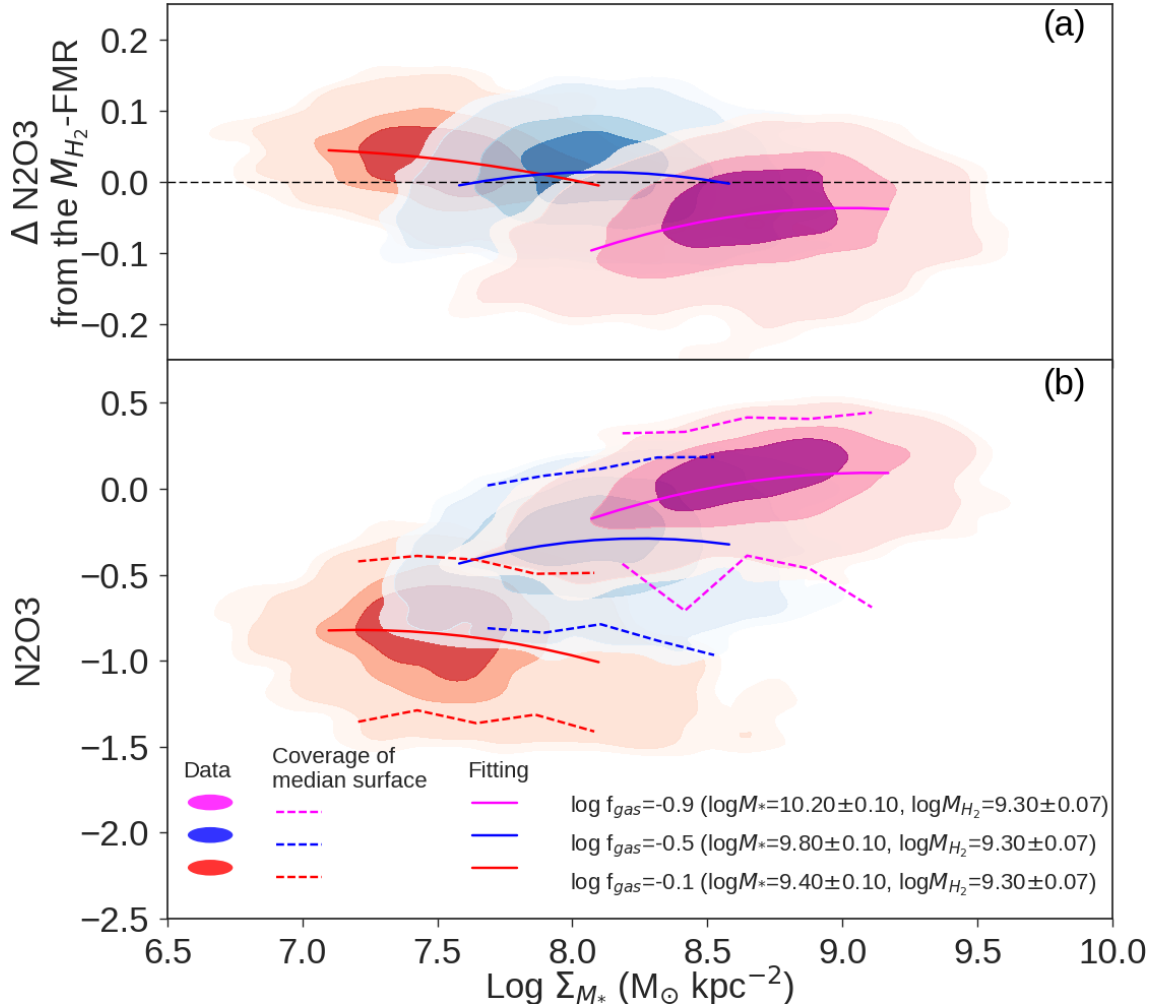


Figure 3. N2O3 dependency on the surface density of stellar mass in the physical scale. **(a)**, N2O3 offset around the molecular-gas FMR, i.e. the 3D relation of stellar mass, N2O3 and molecular-gas mass as a function of surface density of stellar mass. The observed data are sampled from gas-mass-fraction bins. Galaxies with three different gas mass fractions are displayed in magenta, blue and red. Contours contain 38.2%, 68.3%, 95.5% and 99.7% of each binned sample. Solid lines are polynomial fits of each binned sample. Horizontal dashed line corresponds to the surface of the molecular-gas FMR defined by the median distribution of data points in the 3D space. **(b)**, Same as (a) but for N2O3 in the vertical axis. The two dashed lines of each binned sample indicate the coverage of the projected 4D fundamental relation defined by median data points within the binning size of the sampled data. The lower and upper dashed lines are 1 and 99 percentiles of the N2O3 of the sampled galaxies expected from the 4D fundamental relation.

values (0.003 and 0.003-0.005 dex) are well below the typical observational error of N2O3 (0.03 dex). Therefore the effects by uncertainties of SFR and surface density of stellar mass are negligible. The expected N2O3 dispersions (from errors) of both 3D and 4D surfaces are dominated by mass and N2O3 errors.

We tested how the stellar-mass uncertainty affects on the N2O3 offset measurements in the standardised stellar-mass-N2O3 space. Figure 7 is the schematic diagram to show how the offset distances behave when the stellar-mass error changes. In Figure 7, suppose that the true data point (red dot) on the stellar-mass-N2O3 relation can be observed below the relation (black dot) according to the mass error. In the top figure, two N2O3 offsets (red and blue dashed lines) measured by two different ways are within the observational uncertainty of N2O3. However, actual situation in our sample is more similar to the bottom figure in which the stellar-

mass error corresponds to 0.09 dex in physical scale. The red and blue distances can be comparable to or beyond the error of N2O3 depending on how large the mass uncertainty is. In this sense we can not directly compare the observational N2O3 error (0.03 dex) with measured dispersion in N2O3 regardless of these two different ways to measure the offset.

We therefore performed a simple Monte-Carlo simulation to estimate the expected N2O3 dispersion when we assume typical observational errors of N2O3 (0.03 dex) and stellar mass (0.06 - 0.92 dex depending on stellar mass). We generated 1000 true data points (like a red dot in Figure 7) following the best-fit function of the stellar-mass-N2O3 relation (black solid line in Figure 7). At each point on the relation, 1000 artificial observed points are generated which follow the probability distribution function of 2D gaussian with uncertainties of N2O3 and stellar mass (like a black

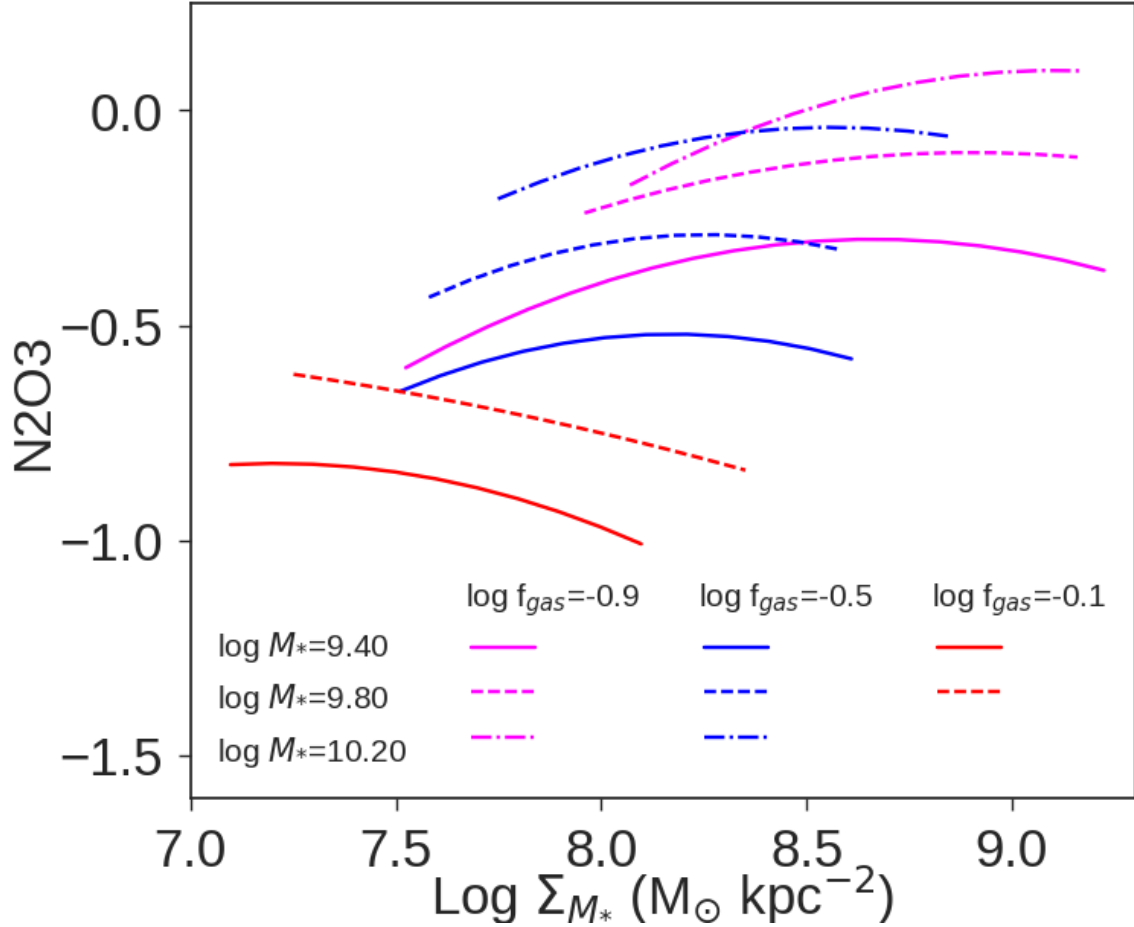


Figure 4. Dependency of the relation between surface density of stellar mass and N2O3 on gas-mass fraction. Galaxies are divided into eight-bin samples with different stellar masses and gas mass fractions. Polynomial fits of the eight-bin samples are shown as lines with different colours and styles, which correspond to the different gas mass fractions and stellar masses, respectively.

dot in Figure 7. Thus, we simulated in total 10^6 N2O3 projections of the orthogonal distance distributed around the stellar-mass-N2O3 relation.

The standard deviation of the simulated N2O3 projections of orthogonal distances is ~ 0.04 dex in N2O3 physical scale as shown in Figure 8, i.e. we expect ~ 0.04 dex dispersion in N2O3 due to the error budgets of N2O3 and stellar mass. The actual dispersion of N2O3 projections of orthogonal distances around the 3D relation (0.07 dex in N2O3 shown in Figure 5) is larger than ~ 0.04 dex, therefore, suggesting a need for the new parameter. This dispersion can be further reduced by introducing a new parameter. Indeed it was reduced to 0.034 dex in our 4D analysis in Figure 5. The expected N2O3 dispersion calculated by Monte-Carlo simulation (~ 0.04 dex) is comparable to the actual dispersion of N2O3 projections of orthogonal distances around the new 4D relation (0.034 dex), which indicates the dispersion around the 4D relation is dominated by the observational errors of N2O3 and stellar mass.

In summary, the new fundamental metallicity relation including the surface density of stellar mass defines a tighter hypersurface in the 4D parameter space.

7 DISCUSSION

7.1 Radial metallicity gradient

A radial gradient of metallicity within a galaxy could cause metallicity to depend on surface density of stellar mass. For example, metallicity is generally lower in the outskirts of a spiral galaxy (Zaritsky et al. 1994). We measured the metallicity of our sample within a fixed SDSS aperture size ($3''.0$ in diameter) to trace more of the outer part for smaller galaxies while concentrating on the central part for larger galaxies. A smaller size of a galaxy corresponds to a higher surface density for a fixed stellar mass. The negative correlation of high- f_{gas} galaxies shown in Figure 3 and 4 could be an aperture effect, but such an effect would probably have little impact for two reasons. Firstly, the measurement of metallicity is, in general, flux weighted and biased towards the central bright region regardless of the size of the galaxy. Secondly, a lower redshift limit ($z > 0.04$) is imposed on the sample to ensure that the metallicity is approximately the same as the global value (Kewley et al. 2005). We tested the surface-density-N2O3 relation based on galaxies that appeared smaller than the spectroscopic aperture size to limit substantially any possible aperture effect. Although this apparent-size limit traces only high-surface-

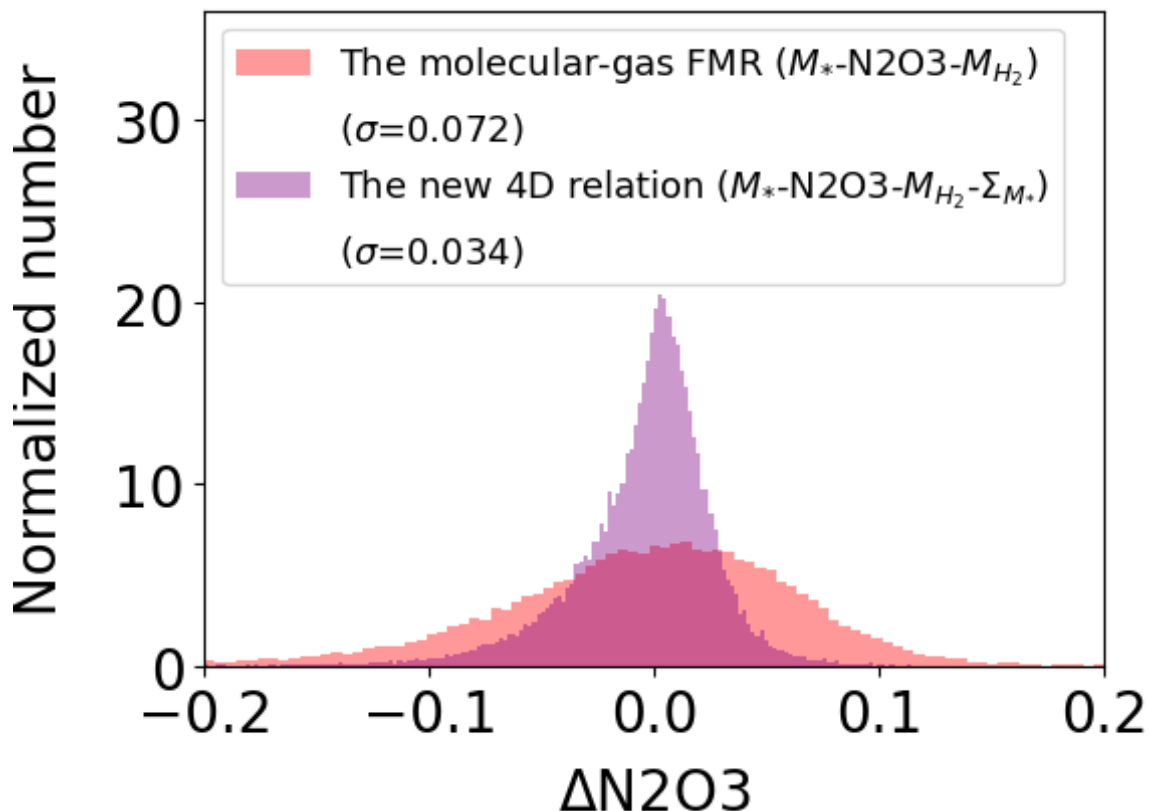


Figure 5. Normalised histograms of N2O3 offsets from the molecular-gas FMR and new 4D relation. Orthogonal distances from these two relations are projected on the N2O3 axis in the physical scale to calculate the N2O3 offset.

density galaxies and so the resulting sample is small, the general trend of the surface-density-N2O3 relations remains the same (Figure 9). Hence, the surface-density-N2O3 relations are unlikely to be attributable to any aperture effect.

7.2 Outflow and inflow

Galactic outflow and inflow are possible candidates for the link between metallicity and surface density of stellar mass. Enriched gas outflow can remove metals from a galaxy, and this process is more effective in the shallower gravitational potentials of less massive galaxies if the wind velocity is roughly constant over the whole range of stellar mass, resulting in the well-known stellar-mass-metallicity relation (Garnett 2002; Tremonti et al. 2004). Suppose that two galaxies with the same stellar mass have almost the same depth of gravitational well, but that the surface gravity depends on the galactic surface density. Galactic wind might easily escape in the case of less concentrated surface gravity on average, thereby giving rise to the surface-density-N2O3 relation. However, cosmological hydrodynamic simulations suggest that such a constant-velocity model disagrees strongly with the observed slope and scatter of the stellar-mass-metallicity relation and that the wind velocity is always high enough to escape the gravitational well (Finlator & Davé 2008). In such a case, the N2O3 dependence of surface gravity should disappear.

Metallicity dilution and star formation caused by inflow of metal-poor gas is another possible candidate. If the dilu-

tion time scale is longer than the dynamical time scale of infall (i.e. $t_{dil} > t_{dyn}$), the galaxy is in the process of returning to the equilibrium metallicity as determined by the dilution and chemical enrichment by newly invoked star formation. Such a galaxy might have observationally lower metallicity compared with the equilibrium metallicity because the bulk of emission lines is emitted from the star-forming regions in metal-poor infall gas. Because the ratio t_{dil}/t_{dyn} is proportional to $\sqrt{\rho}$, where ρ is the mass density (Ellison et al. 2008), galaxies with higher surface mass density may be expected to have larger values of t_{dil}/t_{dyn} , suggesting lower metallicity. This time lag before metallicity dilution is expected to be more evident in gas-rich galaxies that are undergoing active infall and star formation. This is reflected exactly in the negative correlation for high- f_{gas} galaxies shown in Figure 4, whereas the low- f_{gas} galaxies indicate the opposite trend of this metallicity-dilution scenario. The latter type of galaxy is probably in the terminal stage of molecular-gas depletion, which means that its metallicity is already in equilibrium.

7.3 Efficiency

Star-formation efficiency is a likely reasonable explanation for the surface-density-N2O3 relation of low- f_{gas} galaxies. The Schmidt-Kennicutt law indicates that a more concentrated galaxy has a higher SFR compared with the molecular-gas mass, in other words a higher SFR/ M_{H_2} ratio (see APPENDIX A). This means that galaxies with higher surface density are more efficient at turning gas into stars,

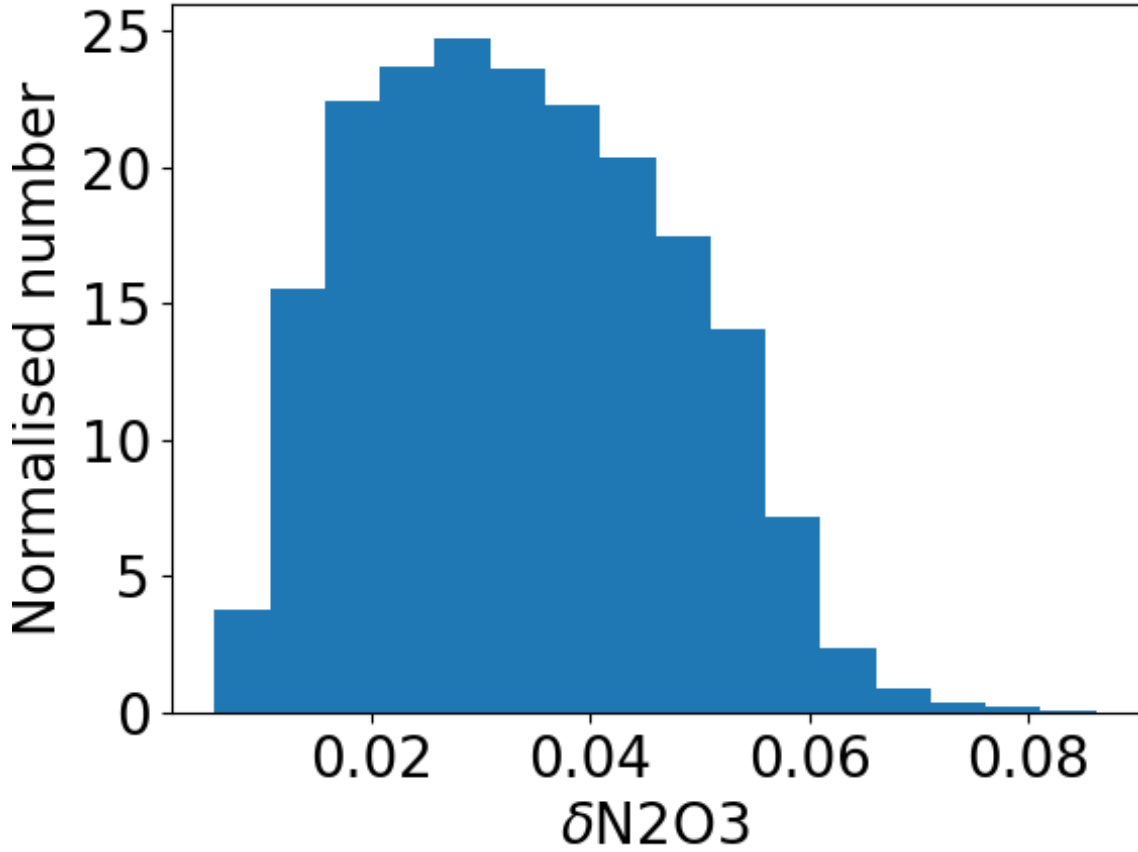


Figure 6. Normalised histogram of observational errors of N2O3 in our sample.

resulting in higher metallicity. This expected trend is consistent with the observed surface-density-N2O3 relation of low- f_{gas} galaxies shown in Figure 4. Star-formation efficiency has been discussed as an alternative to the aforementioned galactic-wind scenario as a means to reproduce the stellar-mass-metallicity relation (Brooks et al. 2007; Dalcanton 2007; Calura et al. 2009). Massive galaxies form stars more effectively and are more chemically evolved than do less massive galaxies, which is known as the ‘downsizing’ formation of galaxies. Such downsizing is related to the total stellar mass of the galaxy. The surface-density-N2O3 relation suggests that galaxies with higher surface density form stars more effectively and are more chemically evolved than do galaxies with lower surface density for a fixed stellar mass.

7.4 Global and local physical parameters

The dilution time scale of gas inflow and the star-formation efficiency could be, to a greater or lesser extent, underlying mechanisms that are common to all star-forming galaxies. The dependence of N2O3 on surface density of stellar mass is probably regulated by a combination of these two mechanisms. The fractional contribution of gas inflow could be greater in high- f_{gas} galaxies, whereas the star-formation efficiency is likely more important in low- f_{gas} galaxies. The relatively gentle slope of galaxies in the mid- f_{gas} bin in Figure 4 may be due to the relatively weak contribution of the gas inflow.

The physical mechanism of SFR and surface density to affect metallicity could be different, although the impact of SFR on the stellar-mass metallicity relation is still in debate (Telford et al. 2016; Kashino et al. 2016; Sánchez et al. 2017; Barrera-Ballesteros et al. 2017). Thus both may exist. However, it is not a focus of our paper to rule out the re-examined results that claim a lack or weaker dependence of SFR on MZR.

The second-order effects of surface density on metallicity likely originate from the local physical conditions of a galaxy. It has been reported recently that the locally defined fundamental relations of star-forming galaxies can, to some extent, reproduce the global properties of the stellar-mass-metallicity relation and the radial metallicity gradient simultaneously by integrating spatially resolved data (Barrera-Ballesteros et al. 2016). The main implication of this is that the local physical properties are closely involved in determining the global metallicity property. The surface density of a galaxy is likely a bridge between such local and global natures. Our findings indicate that it is not sufficient to consider only global relations such as the FMR and molecular-gas FMR. Both global and local parameters are needed to understand the physics of star-forming galaxies. The representative metallicity of a galaxy is regulated by not only global parameters but also local physics such as dilution and star-formation efficiency as traced by the surface density. The surface density of a galaxy is one of the most basic observables, and it will be easily measured in upcoming large imaging surveys such as the Dark Energy Survey (The

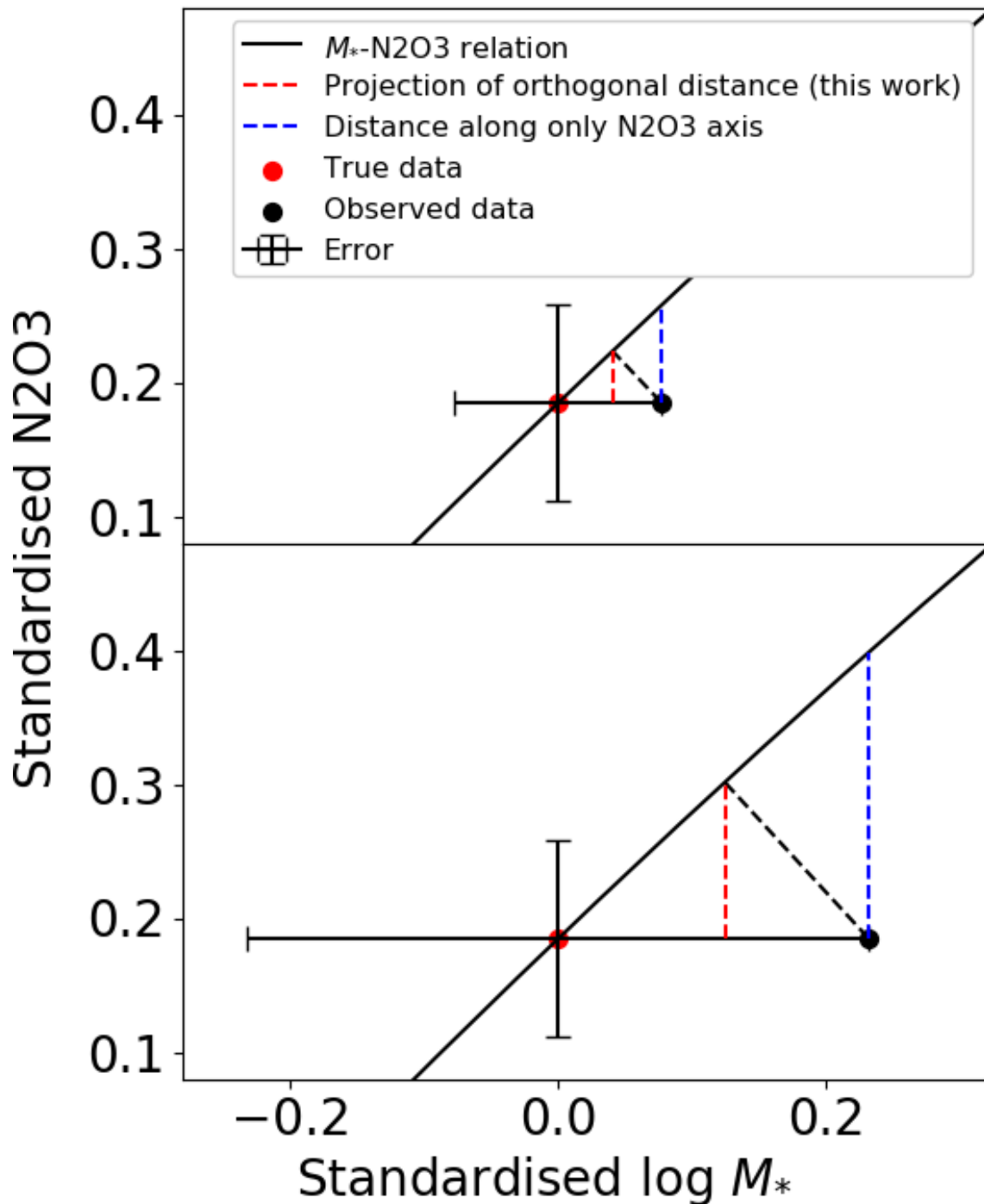


Figure 7. Schematic diagrams of offset measurements in N2O3 axis in cases of small (top) and large (bottom) uncertainties on stellar mass. Red and blue dashed lines show projection of orthogonal distance (this work) and offset measured along only N2O3 axis (previous works). True data point (red dot) on the stellar-mass-N2O3 relation (black solid line) can be observed below the relation according to the observational errors of N2O3 and stellar mass. Note that both axes are standardised. N2O3 error corresponds to 0.03 dex in physical scale. Stellar-mass errors in top and bottom correspond to 0.03 and 0.09 dex in physical scale, respectively.

Dark Energy Survey Collaboration 2005), Hyper Suprime-Cam (Miyazaki et al. 2012) and the Large Synoptic Survey Telescope (Ivezic et al. 2008). We suggest that future FMR studies consider the FMR in 4D space, including the surface density of stellar mass.

8 CONCLUSIONS

We performed PCA on 41,338 star-forming galaxies selected from SDSS Data Release 7. In six groups of physical parameters, stellar mass, N2O3, molecular-gas mass, surface density of stellar mass, dark-matter halo mass and ionization parameter are found to show the highest values of factor

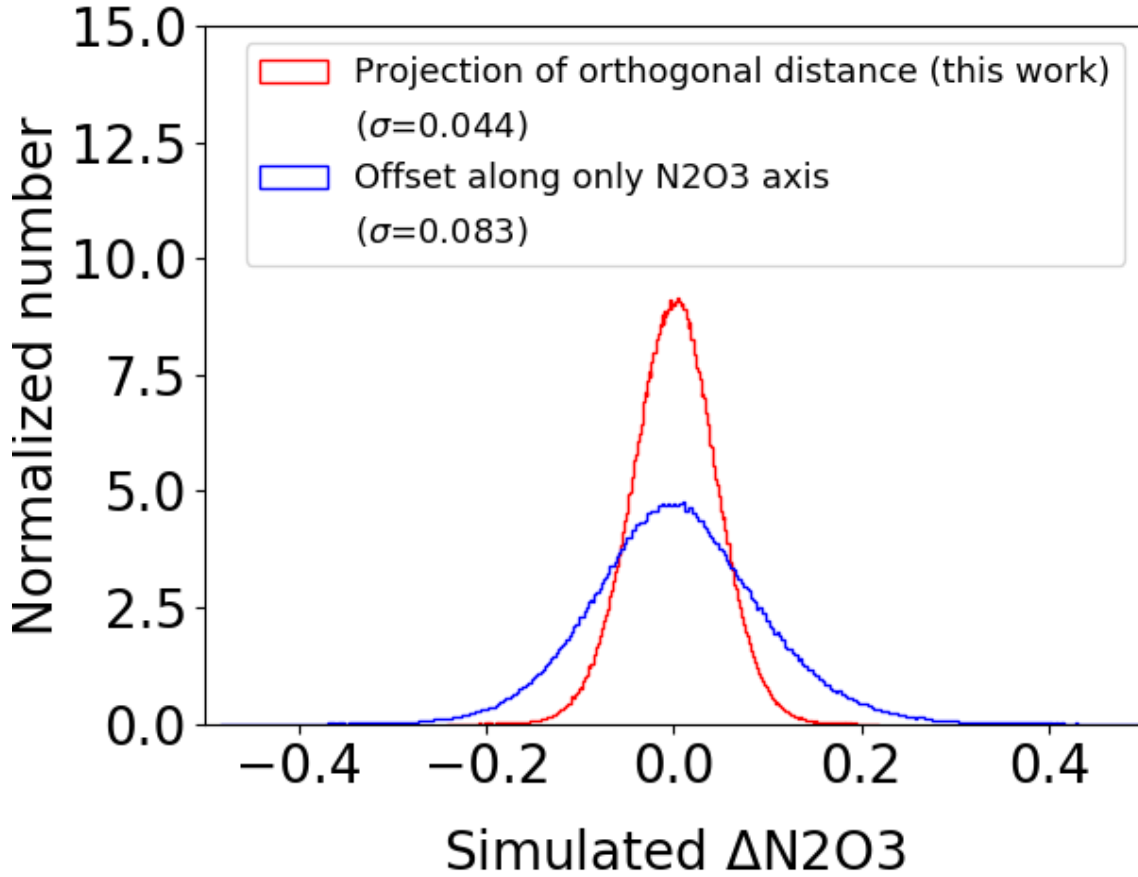


Figure 8. N2O3 dispersions in physical scale expected from typical observational errors of N2O3 and stellar mass based on a Monte-Carlo simulation. Red and blue are histograms of N2O3 projections of orthogonal distances and offsets along only N2O3 axis, respectively.

loadings in the 3D space of PC1-3. Among the combinations of these parameters, the dispersion around the fundamental relation defined by stellar mass, N2O3, molecular-gas mass and surface density of stellar mass is the smallest, which indicates that the fourth most important parameter of star-forming galaxies is the surface density of stellar mass. The reduction of the dispersion by adding the fourth parameter is predominant in N2O3 axis, i.e., the fourth parameter reduces N2O3 dispersion to 50% of that of the molecular-gas FMR. We found that the surface-density-N2O3 relation depending on gas-mass fraction is responsible for the reduction of the dispersion around the fundamental relation. The dilution time scale of gas inflow in gas-rich galaxies and the star-formation efficiency in gas-poor galaxies could explain the observational dependence on surface density. We suggest that future FMR studies consider the FMR in 4D space, including the surface density of stellar mass.

ACKNOWLEDGEMENTS

We thank the anonymous referees for many insightful comments. We are very grateful to Teimoorinia Hossen and Ellison Sara L. for providing a catalogue of physical parameters of SDSS star-forming galaxies. T.G. acknowledges the support by the Ministry of Science and Technology of Taiwan through grant NSC 103-2112-M-007-002-MY3, and 105-2112-M-007-003-MY3.

REFERENCES

- Abazajian K. N., et al., 2009, *ApJS*, 182, 543
 Asplund M., Grevesse N., Sauval A. J., Scott P., 2009, *ARA&A*, 47, 481
 Baldwin J. A., Phillips M. M., Terlevich R., 1981, *PASP*, 93, 5
 Barrera-Ballesteros J. K., et al., 2016, *MNRAS*, 463, 2513
 Barrera-Ballesteros J. K., Sánchez S. F., Heckman T., Blanc G. A., The MaNGA Team 2017, *ApJ*, 844, 80
 Bianco F. B., Modjaz M., Oh S. M., Fierroz D., Liu Y. Q., Kewley L., Graur O., 2016, *Astronomy and Computing*, 16, 54
 Bothwell M. S., Maiolino R., Kennicutt R., Cresci G., Mannucci F., Marconi A., Ciccone C., 2013, *MNRAS*, 433, 1425
 Bothwell M. S., Maiolino R., Peng Y., Ciccone C., Griffith H., Wagg J., 2016a, *MNRAS*, 455, 1156
 Bothwell M. S., Maiolino R., Ciccone C., Peng Y., Wagg J., 2016b, *A&A*, 595, A48
 Brinchmann J., Charlot S., White S. D. M., Tremonti C., Kauffmann G., Heckman T., Brinkmann J., 2004, *MNRAS*, 351, 1151
 Brisbin D., Harwit M., 2012, *ApJ*, 750, 142
 Brooks A. M., Governato F., Booth C. M., Willman B., Gardner J. P., Wadsley J., Stinson G., Quinn T., 2007, *ApJ*, 655, L17
 Bruzual G., Charlot S., 2003, *MNRAS*, 344, 1000
 Bruzual A. G., 1983, *ApJ*, 273, 105
 Calura F., Pipino A., Chiappini C., Matteucci F., Maiolino R., 2009, *A&A*, 504, 373
 Calzetti D., Armus L., Bohlin R. C., Kinney A. L., Koornneef J., Storchi-Bergmann T., 2000, *ApJ*, 533, 682
 Dalcanton J. J., 2007, *ApJ*, 658, 941

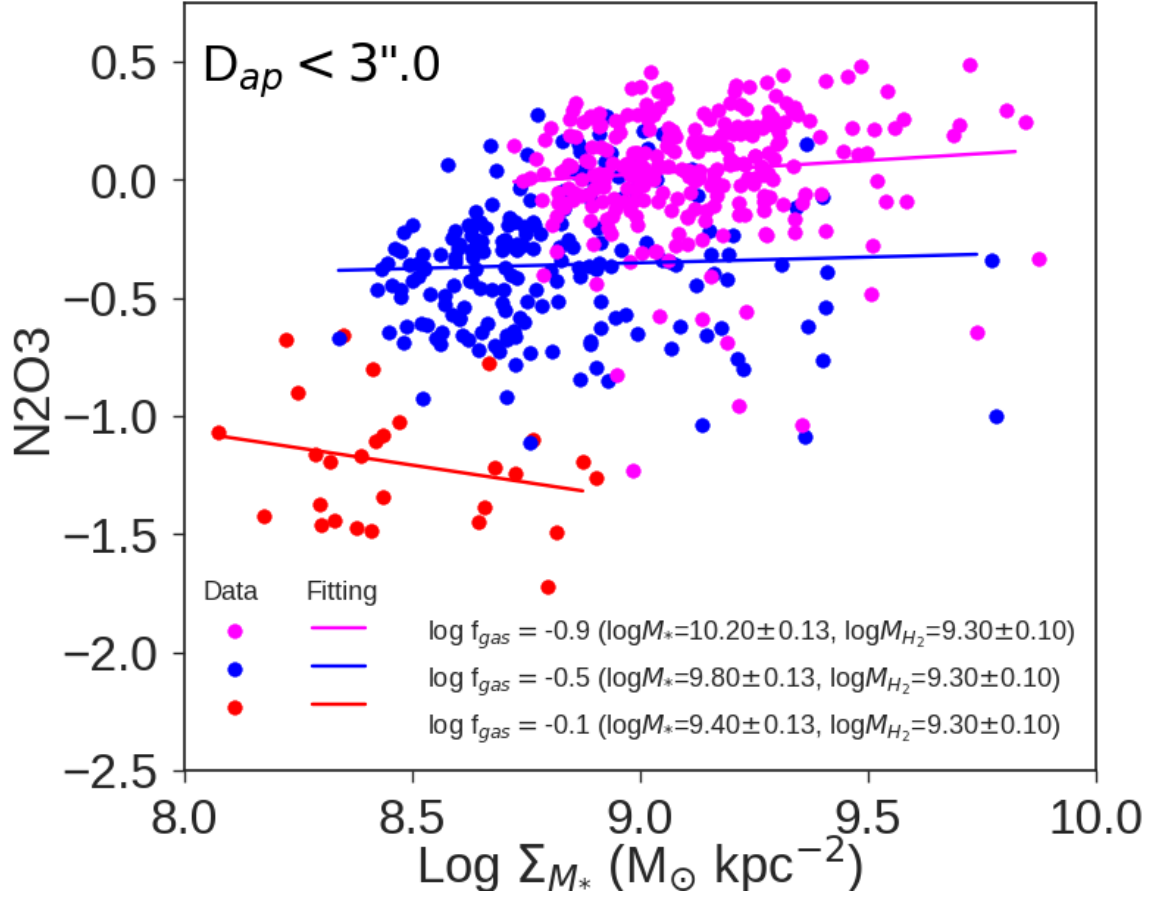


Figure 9. Relations between surface density of stellar mass and metallicity based on apparently small galaxies. Galaxies appearing smaller than the aperture size of SDSS spectroscopic data ($3''.0$ in diameter) are selected to remove the possible aperture effect on metallicity. The binning size is slightly larger than that in Figure 3 to ensure a sufficient sample size. Solid lines indicate the best fits of linear functions for each binned sample.

Denicoló G., Terlevich R., Terlevich E., 2002, MNRAS, 330, 69
 Ellison S. L., Patton D. R., Simard L., McConnachie A. W., 2008, ApJ, 672, L107
 Erb D. K., Shapley A. E., Pettini M., Steidel C. C., Reddy N. A., Adelberger K. L., 2006, ApJ, 644, 813
 Feldmann R., Gnedin N. Y., Kravtsov A. V., 2012, ApJ, 747, 124
 Finlator K., Davé R., 2008, MNRAS, 385, 2181
 Forbes J. C., Krumholz M. R., Burkert A., Dekel A., 2014, MNRAS, 443, 168
 Garnett D. R., 2002, ApJ, 581, 1019
 Ivezić Z., et al., 2008, preprint, (arXiv:0805.2366)
 Kashino D., Renzini A., Silverman J. D., Daddi E., 2016, ApJ, 823, L24
 Kauffmann G., et al., 2003, MNRAS, 346, 1055
 Kennicutt Jr. R. C., 1998, ApJ, 498, 541
 Kewley L. J., Dopita M. A., 2002, ApJS, 142, 35
 Kewley L. J., Ellison S. L., 2008, ApJ, 681, 1183
 Kewley L. J., Jansen R. A., Geller M. J., 2005, PASP, 117, 227
 Kewley L. J., Groves B., Kauffmann G., Heckman T., 2006, MNRAS, 372, 961
 Kobulnicky H. A., Kewley L. J., 2004, ApJ, 617, 240
 Köppen J., Weidner C., Kroupa P., 2007, MNRAS, 375, 673
 Maiolino R., et al., 2008, A&A, 488, 463
 Mannucci F., Cresci G., Maiolino R., Marconi A., Gnerucci A., 2010, MNRAS, 408, 2115
 Marino R. A., et al., 2013, A&A, 559, A114
 McGaugh S. S., 1991, ApJ, 380, 140

Miyazaki S., et al., 2012, in Ground-based and Airborne Instrumentation for Astronomy IV. p. 84460Z, doi:10.1117/12.926844
 Nakajima K., Ouchi M., 2014, MNRAS, 442, 900
 Osterbrock D. E., 1989, Astrophysics of gaseous nebulae and active galactic nuclei
 Pettini M., Pagel B. E. J., 2004, MNRAS, 348, L59
 Pilyugin L. S., Vílchez J. M., Thuan T. X., 2010, ApJ, 720, 1738
 Salim S., et al., 2007, ApJS, 173, 267
 Salim S., Lee J. C., Ly C., Brinchmann J., Davé R., Dickinson M., Salzer J. J., Charlot S., 2014, ApJ, 797, 126
 Salim S., Lee J. C., Davé R., Dickinson M., 2015, ApJ, 808, 25
 Sánchez S. F., et al., 2017, MNRAS, 469, 2121
 Schruba A., et al., 2012, AJ, 143, 138
 Simard L., Mendel J. T., Patton D. R., Ellison S. L., McConnachie A. W., 2011, ApJS, 196, 11
 Teimoorinia H., Ellison S. L., Patton D. R., 2017, MNRAS, 464, 3796
 Telford O. G., Dalcanton J. J., Skillman E. D., Conroy C., 2016, ApJ, 827, 35
 The Dark Energy Survey Collaboration 2005, ArXiv Astrophysics e-prints,
 Tremonti C. A., et al., 2004, ApJ, 613, 898
 Wolfire M. G., Hollenbach D., McKee C. F., 2010, ApJ, 716, 1191
 Yabe K., et al., 2014, MNRAS, 437, 3647
 Yang X., Mo H. J., van den Bosch F. C., Pasquali A., Li C., Barden M., 2007, ApJ, 671, 153

Yang X., Mo H. J., van den Bosch F. C., 2009, ApJ, 695, 900
 Zaritsky D., Kennicutt Jr. R. C., Huchra J. P., 1994, ApJ, 420, 87
 de los Reyes M. A., et al., 2015, AJ, 149, 79

APPENDIX A: PHYSICAL PARAMETERS OF STAR-FORMING GALAXIES

In total, 18 physical parameters of 41,338 galaxies were compiled from various literature sources, and a further 11 were calculated in this work. Logarithms in physical parameters were taken before standardization. We summarise the details of all 29 parameters below.

- M_* (M_\odot), Stellar mass was collected from the publicly available MPA/JHU catalogue, in which galaxy-population-synthesis models (Bruzual & Charlot 2003) are fitted to multi-band photometric data to estimate stellar mass. Standardised log M_* was used in the PCA.

- M_{virial} (M_\odot), Virial mass was estimated as $2r_{\text{half}}\sigma^2/G$. r_{half} and σ are r -band half-light radius and rest-frame velocity dispersion, respectively. G is gravitational constant. Standardised log M_{virial} was used in the PCA.

- σ (km s^{-1}), Rest-frame velocity dispersion was collected from the MPA/JHU catalogue. Standardised log σ was used in the PCA.

- M_{igas} (M_\odot), Ionised-gas mass was estimated as $2.33 \times 10^3 (L_{\text{H}\alpha} / 10^{39} \text{ erg s}^{-1}) (10^3 \text{ cm}^{-3} / n_e) M_\odot$ under the assumption of case B recombination (Osterbrock 1989). $L_{\text{H}\alpha}$ and n_e are $\text{H}\alpha$ luminosity and electron density, respectively. Standardised log M_{igas} was used in the PCA.

- M_u, M_g, M_r, M_i, M_z , Absolute magnitudes in u, g, r, i and z bands as collected from the literature (Teimoorinia et al. 2017). Standardised M_u, M_g, M_r, M_i and M_z were used in the PCA.

- N2O3, Metallicity indicator was calculated as $\text{N2O3} = \log\left(\frac{[\text{N II}]\lambda 6584/\text{H}\alpha}{([\text{O III}]\lambda 5007/\text{H}\beta)}\right)$. N2O3 can be converted to metallicity through $12 + \log(\text{O}/\text{H}) = 8.73 + 0.32 \times \text{N2O3}$ based on the PP04O3N2 method with an uncertainty of ~ 0.14 dex (Pettini & Pagel 2004). In addition, 14 other metallicity calibrations (Denicoló et al. 2002; Zaritsky et al. 1994; McGaugh 1991; Pettini & Pagel 2004; Pilyugin et al. 2010; Maiolino et al. 2008; Marino et al. 2013; Kewley & Dopita 2002; Kobulnicky & Kewley 2004; Kewley & Ellison 2008) were examined to confirm the universality of the surface-density-metallicity relation by using a metallicity calculation code (Bianco et al. 2016). The same trend of the surface-density-metallicity relation shown in Figure 4 comes out in all of these metallicity calibrations. Standardised N2O3 was used in the PCA.

- M_{metal} (M_\odot), Metal mass in ionised gas was calculated as $10^{12 + \log(\text{O}/\text{H}) - 8.69} \times 0.0181 \times M_{\text{igas}}$, where the factors of 8.69 and 0.0181 are the solar oxygen abundance and metal mass ratio, respectively (Asplund et al. 2009). Standardised log M_{metal} was used in the PCA.

- A_V , V-band dust extinction was calculated from the observed Balmer decrement ($\text{H}\alpha/\text{H}\beta$) assuming the extinction law of star-forming galaxies (Calzetti et al. 2000). Standardised A_V was used in the PCA.

- SFR ($M_\odot \text{ yr}^{-1}$), Star-formation rate was collected from the MPA/JHU catalogue, in which SFR is calculated from

$\text{H}\alpha$ luminosity corrected for dust extinction and aperture loss (Brinchmann et al. 2004). Standardised log SFR was used in the PCA.

- sSFR (yr^{-1}), Specific SFR was calculated as SFR/M_* . Standardised log sSFR was used in the PCA.

- $\text{EW}_{\text{H}\alpha}$ (\AA), Rest-frame equivalent width was collected from the MPA/JHU catalogue. Standardised log $\text{EW}_{\text{H}\alpha}$ was used in the PCA.

- D4000, Index of 4000- \AA break was collected from the MPA/JHU catalogue. D4000 is defined as $\langle F^+ \rangle / \langle F^- \rangle$, where $\langle F^+ \rangle$ and $\langle F^- \rangle$ are flux densities averaged over 4050-4250 \AA and 3750-3950 \AA (Bruzual A. 1983). Standardised log D4000 was used in the PCA.

- $g-r$, Colour of $g-r$ was collected from the literature (Teimoorinia et al. 2017). Standardised $g-r$ was used in the PCA.

- M_{HI} , Atomic hydrogen gas mass was collected from the literature (Teimoorinia et al. 2017). It has been reported that M_{HI} can be estimated empirically from the combination of 15 physical parameters of a star-forming galaxy (Teimoorinia et al. 2017), although the physical mechanism underlying this relation is still open to debate. Standardised log M_{HI} was used in the PCA.

- M_{H_2} , Molecular-gas mass was estimated assuming the Schmidt-Kennicutt law (Kennicutt 1998), which is an empirical relation between surface density of SFR and molecular-gas mass, i.e. $\Sigma_{\text{SFR}} = 1.6 \times 10^{-4} (\Sigma_{\text{gas}} / M_\odot \text{ pc}^{-2})^{1.4} M_\odot \text{ yr}^{-1} \text{ kpc}^{-2}$. This relation is equivalent to $M_{\text{gas}} \propto (\text{SFR})^{5/7} (\pi r^2)^{2/7}$. Therefore, the molecular-gas mass can be calculated from the SFR and the size of the galaxy by assuming this relation. The Schmidt-Kennicutt law can also be expressed as $\text{SFR}/M_{\text{gas}} \propto (\Sigma_{\text{gas}})^{0.4} = (f_{\text{gas}} \Sigma_{M_*})^{0.4}$, which indicates a higher star-formation efficiency in a more concentrated galaxy. Standardised log M_{H_2} was used in the PCA. Although the derivations of the above two gas masses are not direct methods, they are included in the analyses to estimate the importance of gas mass.

- r_{disk} (kpc), Exponential disk scale length was collected from the literature (Teimoorinia et al. 2017). Galaxy structural parameters were measured from bulge+disk decompositions, i.e. a pure exponential disk and de Vaucouleurs bulge (Simard et al. 2011). Standardised log r_{disk} was used in the PCA.

- r_{half} (kpc), Half-light radius along a semi-major axis in r -band (Simard et al. 2011) was collected from the literature (Teimoorinia et al. 2017). Standardised log r_{half} was used in the PCA.

- Σ_{M_*} ($M_\odot \text{ kpc}^{-2}$), Surface density of stellar mass was calculated as $M_*/\pi r_{\text{half}}^2$. Standardised log Σ_{M_*} was used in the PCA.

- Σ_{SFR} ($M_\odot \text{ yr}^{-1} \text{ kpc}^{-2}$), Surface density of SFR was calculated as $\text{SFR}/\pi r_{\text{half}}^2$. Standardised log Σ_{SFR} was used in the PCA.

- B/T, Bulge-to-total fraction in r -band was collected from the literature (Teimoorinia et al. 2017). This fraction is based on a pure exponential disk and de Vaucouleurs bulge decompositions (Simard et al. 2011). Standardised B/T was used in the PCA.

- δ_5 , Local galaxy number density was collected from the literature (Teimoorinia et al. 2017) and is defined as $\Sigma_n = n/\pi d_n^2$ (here, $n=5$). d_n is the projected distance in Mpc

to the n -th nearest neighbour within $\pm 1000 \text{ km s}^{-1}$. δ_5 is normalized by the median Σ_n within a redshift slice of ± 0.01 . Standardised $\log \delta_5$ was used in the PCA.

- M_{halo} (M_\odot), Mass of dark-matter halo hosting galaxies was collected from the literature (Teimoorinia et al. 2017). The halos were identified in previous work (Yang et al. 2007, 2009). Standardised $\log M_{halo}$ was used in the PCA.

- n_e (cm^{-3}), Electron density was calculated from the line ratio of $[\text{S II}]\lambda 6717/[\text{S II}]\lambda 6731$ assuming an electron temperature of 10^4 K. In cases in which the ratio was beyond the theoretical asymptotic values (Osterbrock 1989), $[\text{O II}]\lambda 3729/[\text{O II}]\lambda 3726$ was used instead. If both were out of range, $[\text{S II}]\lambda 6717/[\text{S II}]\lambda 6731$ was replaced with the asymptotic values of ~ 1.4 or 0.5 . Standardised $\log n_e$ was used in the PCA.

- q , Indicator of ionisation parameter was calculated as $[\text{O III}]\lambda 5007/[\text{O II}]\lambda 3727$ corrected for dust extinction. Standardised $\log [\text{O III}]\lambda 5007/[\text{O II}]\lambda 3727$ was used in the PCA.

- z , Redshift was collected from the MPA/JHU catalogue. Standardised $\log z$ was used in the PCA.

APPENDIX B: FACTOR LOADING OF PCA

Because various measurements with different units are used simultaneously in the PCA, all data were standardised for a fair comparison. The standardised parameter X_{std}^i is defined as $X_{std}^i = (X^i - X_{ave}) / \sigma_X$, where X^i is an original parameter of the i -th galaxy. X_{ave} and σ_X are the average and standard deviation, respectively, of parameter X .

PCA is a linear transformation of the original parameters. The vector of the new axes, namely, $\vec{PC} = (\text{PC1}, \text{PC2}, \dots, \text{PC}n)$, can be expressed as $\vec{PC} = A \cdot \vec{X}$, where \vec{X} is the vector of original parameters. The fractional contributions of original parameters to each new axis $\text{PC}n$ are $\vec{a}_n = (a_{n1}, a_{n2}, \dots, a_{nn})$, which are the n -th-row components of the matrix A . The contribution of the $\text{PC}n$ axis to the total dispersion is proportional to the eigenvalue of $\text{PC}n$ (l_n). Therefore, the factor loadings defined as $\sqrt{l_n} \vec{a}_n$ indicate the contribution of each original parameter to the total dispersion.

This paper has been typeset from a $\text{T}_\text{E}\text{X}/\text{L}^\text{A}\text{T}_\text{E}\text{X}$ file prepared by the author.